Laser-Induced Structuring of Biocompatible Polymers for the Controlled Orientation of Multinucleated Myotubes

Clarissa Murru, Lucas Duvert, Daniel Ferry, Ahmed Al-kattan, Frederique Magdinier, Anne-patricia Alloncle, Stefano Testa, Adrien Casanova

ADVANCED MATERIALS INTERFACES
Open Access
www.advmatinterfaces.de

Laser-Induced Structuring of Biocompatible Polymers for the Controlled Orientation of Multinucleated Myotubes

Clarissa Murru, Lucas Duvert, Daniel Ferry, Ahmed Al-Kattan, Frederique Magdinier, Anne-Patricia Alloncle, Stefano Testa, and Adrien Casanova**

Surface topography plays a critical role in regulating cellular behavior through contact guidance. In this context, micro-nanostructured materials have gained widespread use in biomedicine with applications in biosensing, bioimaging, or tissue engineering. Among the different strategies that can be applied for surface structuration, laser-induced surface patterning offers a precise and versatile alternative to traditional lithographic techniques by enabling rapid processing and tailored modifications of material properties. Using an ultrafast femtosecond laser, the laser structuring of three different biopolymers, sodium alginate, gelatin, and collagen are investigated here. The resulting surfaces are analyzed using confocal and scanning electron microscopy (SEM). In parallel, the structural and chemical modifications induced by the laser ablation are thoroughly characterized. The interaction of human myoblasts cultured on these engineered surfaces is evaluated revealing that the laser-induced topographical features have a significant impact on myoblast alignment. Specifically, optimal channel widths of 20–25 µm and interline spacings ranging from 35 to 150 µm promoted efficient cell organization mimicking the native constraint of skeletal muscle tissue. These findings emphasize the potential of laser-patterned polymer surfaces to guide muscle cell orientation and differentiation, providing a promising approach for developing functional surfaces in skeletal muscle tissue engineering.

1. Introduction

In vivo, cell behavior is influenced among others by the physical properties of the extracellular matrix (ECM) and its associated mechanical cues.[1,2] In vitro, cell-to-surface interactions modulate cell morphology, cytoskeletal organization, and gene expression (cit.3). Cell adhesion plays a critical role in cell survival and fate determination (cit.4). In recent years, surface properties, including topography, stiffness, and chemical composition, have been shown to profoundly affect cellular processes by providing both mechanical and biochemical signals that regulate cell response.[5] Recent developments in materials science and tissue engineering have highlighted the crucial role of surface topography in precisely controlling cellular functions. In particular, structural features, such as surface roughness, geometric patterns, and porosity, are recognized by cells via mechanotransduction pathways.[6,7] Multiple studies

C. Murru
National Institute of Optics
National Research Council (INO-CNR)
Sesto Fiorentino 50019, Italy
L. Duvert, A. Al-Kattan, A.-P. Alloncle, A. Casanova
Laser
Plasmas et Procédés Photoniques (LP3)
Centre National de la Recherche Scientifique (CNRS)
Campus de Luminy
Aix-Marseille University
Marseille 13009, France
E-mail: adrien.casanova@univ-amu.fr

L. Duvert, F. Magdinier, S. Testa
Marseille Medical genetics (MMG)
Institut national de la santé et de la recherche médicale (INSERM)
Aix-Marseille University
Marseille 13005, France
E-mail: stefano.testa@univ-amu.fr
D. Ferry
Centre Interdisciplinaire de Nanoscience de Marseille (CINaM)
Centre National de la Recherche Scientifique (CNRS)
Campus de Luminy
Aix-Marseille University
Marseille 13009, France

The ORCID identification number(s) for the author(s) of this article can be found under https://doi.org/10.1002/admi.202500131

DOI: 10.1002/admi.202500131

have demonstrated that micro- and nano-patterned surfaces with specific geometries can significantly affect cell adhesion,[8] increase the orientation,[9,10] and promote the proliferation[11] and differentiation of several lines of cells.[12]

The design of surface patterns can be realized through a range of advanced techniques, each offering unique capabilities for achieving specific structural and functional features.[13–18] For instance, Casanova et al. described a self-aligning chemical functionalization method that enables the creation of low-density neuronal networks with precise control over soma positioning and dendritic growth on aligned nanostructures, allowing for accurate monitoring of neuronal activity at the single-cell level.[19] In contrast, lithography-based approaches are more commonly employed to fabricate highly precise and complex 3D structures.[20,21] Despite the high spatial resolution achieved through lithography, its applicability is limited by several factors, including the significant costs associated with the materials required for pattern generation,[22] and the complexity of the fabrication process[23] which requires specific environmental conditions (vacuum, clean room).[24] In this context, laser-induced topography, as a direct writing and digital process, appears as an opportunity to process a wide range of materials in a simple and efficient way. By enabling the design of 3D structures, laser-induced topography overcomes the limitations of complex traditional lithography and avoids the use of cell-interactive chemicals. The use of high repetition rate lasers allows the rapid processing of a large number of samples under standard environmental conditions. The process is also environmentally friendly as it does not require nor produce chemical pollutants.[25] Laser-based approaches for the design of bio-interfaces range from additive approaches (Matrix Assisted Pulsed Evaporation MAPLE or Laser-Induced Forward transfer LIFT),[26,27] laser direct writing (two photons polymerization to create 3D scaffolds at a nanoscale[28,29] or LIPSS formation) or laser texturing techniques.[30] These last methods rely on the ability to induce localized deformation or ablation of the targeted substrate in one straightforward step under a laser beam irradiation. Modification of the material can here be induced through photothermal and/or photochemical processes, depending on laser parameters (wavelength and pulse duration) and the composition of the substrate (optical properties).

The use of ultrafast lasers has become increasingly popular in recent years thanks to their unique ability to interact with a wide range of materials.[31] Given the transparency of most bio-polymers in the visible and near-infrared range, femtosecond laser pulses provide the high-intensity energy needed to induce non-linear absorption.[32] This enables precise processing of the material at micro and submicron scale levels, on a large range of structures (pillars, ripples, spikes, and grooves) providing a unique control over the uniformity and regularity of the structured surfaces and allowing their use in tissue engineering applications.[25] The ability of laser-structured surfaces to influence cell behavior via topographic guidance has been largely studied;[24,33,34] Dinca et al. reported that the precise control of surface topography can regulate the differentiation and proliferation of various mesenchymal stem cell lineages.[23] Similarly, Angelaki et al. observed that the same topographical patterns elicit distinct responses for peripheral nervous system cells (murine Schwann (SW10) and Neuro2a (N2a) cells), either facilitating or inhibiting their adhesion.[35] These findings question the potential of laser-structured surfaces for modeling skeletal muscle, a tissue characterized by a highly organized anisotropic architecture consisting of parallel and aligned myofibers arranged in bundles.[36] The unidirectional arrangement of these myofibers is crucial for generating efficient contractile force and ensuring functionality.[37] For these reasons, the alignment of myoblasts, precursor cells that fuse to form multinucleated myotubes, which subsequently develop into myofibers in culture is essential for the proper formation of skeletal muscle tissue in vitro.

This work introduces an innovative approach for controlling skeletal muscle cell alignment using ultrafast laser-induced surface structuring of biopolymers. Through precise laser modification, anisotropic topography gradients were created on three widely used biopolymers: i) alginate, known for its biocompatibility and use in controlled drug delivery and skin repair;[38,39] ii) gelatin, a versatile polypeptide that can easily form hybrid biomaterials due to its functional groups[40–42] and iii) collagen, a fundamental structural protein extensively used in the engineering of nerve, musculoskeletal tissues, and vascular grafts.[43–46] A significant breakthrough is the fabrication of microscale channels (20–25 µm wide) with adjustable interline spacings (ranging from 35 to 150 µm), allowing precise tailoring of surface features. This advanced surface structuring approach offers an effective method to influence cellular behavior, specifically enhancing the organization and alignment of human myoblasts, to mimic the natural skeletal muscle tissue architecture.[47] By combining ultrafast laser technology with biopolymer engineering, this work not only deepens the understanding of cell-material interactions but also offers a scalable and adaptable system for designing biomimetic surfaces. The described process could pave the way for the development of advanced and easily accessible engineered culture surfaces, with applications ranging from skeletal muscle modeling and neuromuscular disease studies to personalized and regenerative medicine.

2. Experimental Section

2.1. Coatings Preparation

Sodium alginate (ThermoFisher Scientific) and gelatin powder (Acros Organics) were suspended in deionized water at a concentration of 3% w/v, and the dissolution process of the polymers was optimized by stirring the mixtures for 2 h at 60 °C. A volume of 400 µL was finally cast onto a round glass coverslip with a diameter of 17 mm with a graduated pipette. For the sodium alginate coating, the coverslips were dipped in a 0.5 M $CaCl_2$ solution (ionic cross-linking agent) to promote its reticulation: several tests were carried out by soaking the sodium alginate coatings in $CaCl_2$ for different durations, and the time of 1 min was chosen for subsequent experiments. Gelatin coatings were left to dry at room temperature overnight. The collagen mixture was prepared as follows: 715 µL of a 0.3 mg mL^{-1} solution of collagen was mixed with 85 µL of 10x PBS and 184 µL of cell culture medium (DMEM). Finally, 16 µL of a NaOH solution 1 M was added to promote the gelation of the polymer and reach the final volume of 1 mL. The manipulation of the mixture was carried out while keeping all reagents on ice in order to avoid premature gelling of the collagen. 400 µL were cast onto round glass coverslips to obtain the coatings that spontaneously reticulated after 15 min.

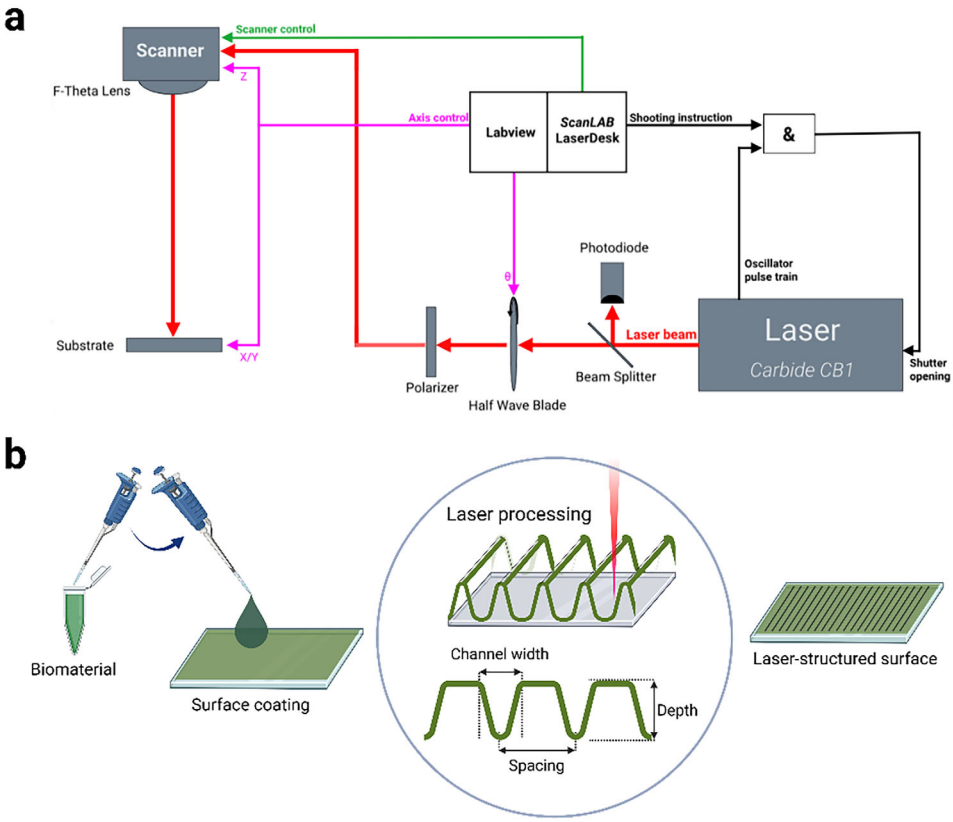

Figure 1. a) Experimental laser set-up for the micro-structuration of polymer samples. b) Preparation protocol of the samples.

2.2. Experimental Set-Up for the Micro-Structuration of Polymer Samples

A 60 kHz femtosecond laser (Carbide CB-01 Light Conversion) emitting at a fundamental wavelength of 1030 nm with an average pulse duration of 213 fs and a maximum power output of 5 W was used to create the micro-structuration. To achieve high processing speed, a galvanometric scanning system (ScanLab intelliSCAN14) coupled with a 70 mm focus length F-Theta lens (Linos F-Theta-Ronar lenses) was used (**Figure 1**). The beam waist, determined by Liu's regression technique,[48] was calculated to be 2wo = 36 µm. The average fluence values will be calculated using this value. Biopolymer surfaces were ablated at a fluence of 0.8J cm^{-2} and at a scan speed of 320 mms^{-1}, corresponding to a pulse overlap of 80%.

With these parameters, the typical channel width ranged from 20 to 25 µm, depending on the processed material. This value was strongly influenced by the beam quality, size, and wavelength. To maximize process speed and efficiency–particularly given the density of topographic features–a high-speed galvanometric scanner was used. Higher processing resolution could be achieved with specialized magnification optics, though at the expense of speed and overall efficiency. The round glass coverslips coated with the different biopolymers were laser-structured to produce micropatterned surfaces (area of 227 mm^2) consisting of arrays of lines with a spacing ranging from 35 to 150 µm. Then, the micro-structured substrates were washed three times in a 70% ethanol solution and rinsed with sterile PBS to ensure sterility for subsequent cell culture experiments.

The patterns created on the surface of the coatings were observed in detail using SEM (JEOL JSM-6390, Tokyo, Japan) and characterized with a confocal microscope (LEICA DCM3D, Nanterre, France).

2.3. Infrared Analysis

The surface chemistry and thermal behavior of the structured samples were recorded in Attenuated Total Reflectance (ATR, germanium crystal) mode using a Bruker VERTEX70 mid-IR Fourier Transform spectrometer equipped with a temperature-stabilized DLaTGS detector (Deuterated lanthanum α-alanine-doped triglycine sulphate). All spectra were accumulated on the surface of the different areas in a spectral range of 650–4000 cm^{-1} by recording 200 scans at a resolution of 4 cm^{-1}.

2.4. Contact Angle Analysis

Wettability modifications of the laser-structured surface were characterized by studying contact angles. Five µL of distilled water was deposited on the created topography and photographed through a camera (DAHUA) equipped with a 10X zoom lens (Computar). The droplets were illuminated by a white light (Wild

Heerbrugg). The angle formed between the surface and the tangent to the droplet surface along their line of contact was calculated using the Contact Angles plugin for FIJI software.[49] The obtained value was used as an index of hydrophobicity: values ranging from 0° to 90° indicate a hydrophilic surface, while values comprised between 90° and 180° a hydrophobic one.

2.5. Cell Cultures

Human immortalized myoblasts were cultured according to a previously published protocol[47] on 10 cm culture dishes (Falcon) at 37 °C with 5% CO_2 in Basal Medium (BM) composed of 4:1 volumes parts of Dulbecco's modified Eagle medium (DMEM, Gibco) and 1 volume of Medium 199 (Gibco), supplemented with 15% fetal bovine serum (Euroclone); 0.02 M HEPES buffer (Invitrogen); 1.4 mg L^{-1} vitamin B12 (Sigma); 0.03 mg L^{-1} ZnSO4 (Fisher Scientific), 0.055 mg L^{-1} dexamethasone (Sigma), 2.5 µg L^{-1} hepatocyte growth factor (Chemicon International) and 10 µg L^{-1} basic fibroblast growth factor (BioPioneer). Once 90% confluency was reached, cells were transferred to Differentiation Media (DM) composed of BM supplemented with 2% Horse Serum (Gibco) to induce final differentiation. For biological experiments, cells were seeded on top of the different micropatterned coated supports at a concentration of 5×10^4 cells per support and grown depending on experimental needs: 3 days of incubation for myoblast-surface interaction experiments and 7 days (3 days in culture medium and 4 days in differentiation medium) for myotubes orientation experiments.

To clearly visualize the cells and to monitor their interactions with the surfaces, samples were incubated with calcein-AM live staining solution (Thermofisher) for 30 min at 37 °C.

Imaging analyses were performed with a reverse microscope (EVOS M5000, Invitrogen, ThermoFisher) and a reverse fluorescence microscope (Axio Observer Z1/7, Zeiss).

2.6. Cell Fixation and Immunofluorescence Analysis

The samples were fixed in paraformaldehyde (4%, for 15 min at 4 °C), washed in PBS, and stored at 4 °C. Immunofluorescence was performed as previously described.[50] Briefly, cells were permeabilized in a solution of Triton X-100 (Sigma) 0.3% in PBS for 1 h at room temperature (RT) and blocked with a blocking solution consisting of 10% natural goat serum (Thermo Fisher Scientific), 1% glycine (Thermo Fisher Scientific), and 0.1% Triton X-100 in PBS for 1 h at RT. Subsequently, the cells were incubated with rabbit polyclonal anti-Desmin (Abcam) primary antibody, diluted 1:100 in blocking solution for 2 h at RT, and then rinsed with a washing solution consisting of 1% bovine serum albumin (BSA, Sigma) and 0.2% Triton X-100 in PBS. After washing, the cells were incubated with Alexa Fluor 488-conjugated goat anti-rabbit IgG secondary antibody (H + L; Thermo Fisher Scientific, diluted 1:400) for 1 h. Finally, the nuclei were counterstained with 300 nM DAPI (Thermo Fisher Scientific) in PBS for 10 min.

2.7. Image Analysis

Once myoblasts were differentiated into myotubes expressing Desmin, their organization was studied using the *OrientationJ* plugin[51] of the Fiji software.[52] In particular, the pictures (832×832 mm^2) were converted into highly contrasted 8-bit images and processed using *the OrientationJ distribution* tool to obtain a weighted histogram of muscle elements orientations; the "weight" of this distribution was represented by the coherency value, a value ranging between 0 (no orientation) and 1 (perfect orientation) calculated using *OrientationJ dominant direction* tool.[53]

2.8. Statistical Analysis

All experiments were performed in biological triplicates. Data were analyzed using GraphPad Prism 8, and values were expressed as means ± standard error. Statistical significance was tested using one-way ANOVA with the appropriate multiple comparison tests. A probability of less than 5% ($P < 0.05$) was considered statistically significant.

3. Result and Discussion

3.1. Morphological Characterization

The aligned patterning obtained on the surface of the polymers was characterized by SEM. The 50 µm spaced channels showed a homogeneous and compact structure, with a width of 20 µm for sodium alginate (**Figure 2a**) and 25 µm for gelatin and collagen (Figure 2b,c) coatings. These dimensions were selected according to the myoblast cells that feature an observed mean dimension of 20 µm.[54] For the different biomaterials, a difference in the morphology and the porosity of the channel surface was observed (Figure 2d–f).

3.2. Characterization of Functional Groups

In the second step, the functional groups were studied both in laser-treated and untreated samples through Fourier-transform infrared spectroscopy (FT-IR). Sodium alginate spectra showed stretching vibrations of Oxygen—Hydrogen (O—H) bonds in the range of 3000–3600 cm^{-1} while stretching vibrations of aliphatic Carbon—Hydrogen (C—H) were observed at 2900–2800 cm^{-1} (Figure 2g–i). The increase in the peak intensity at 1635 cm^{-1} corresponds to the symmetrical stretching of COO-while the peaks observed at 1580, 1416, and 1340 cm^{-1} are attributed to the asymmetrical stretching of the COO— group. Peaks at 1110 and 1034 cm^{-1} are associated with the stretching of the C—O group. In the case of gelatin, both spectra showed similar patterns, and four regions were observed: 3600–2300 cm^{-1}(Amide A), 1656–1644 cm^{-1} (Amide I), 1560–1335 cm^{-1} (Amide II) and 1240–670 cm^{-1} (Amide III). Collagen absorption bands can be distinguished in the amide I at 1657 cm^{-1} resulting from the stretching vibration of the peptide carbonyl group C═O, amide II at 1560 cm^{-1} that corresponds to a combination of the N—H in-plane bend, and the C—H stretch and a set of three weaker bands that represent amide III vibration modes centered at 1245 cm^{-1} belonging to a combination of the C—N stretch and the N—H in-plane bend. Moreover, the absorption registered between 1360

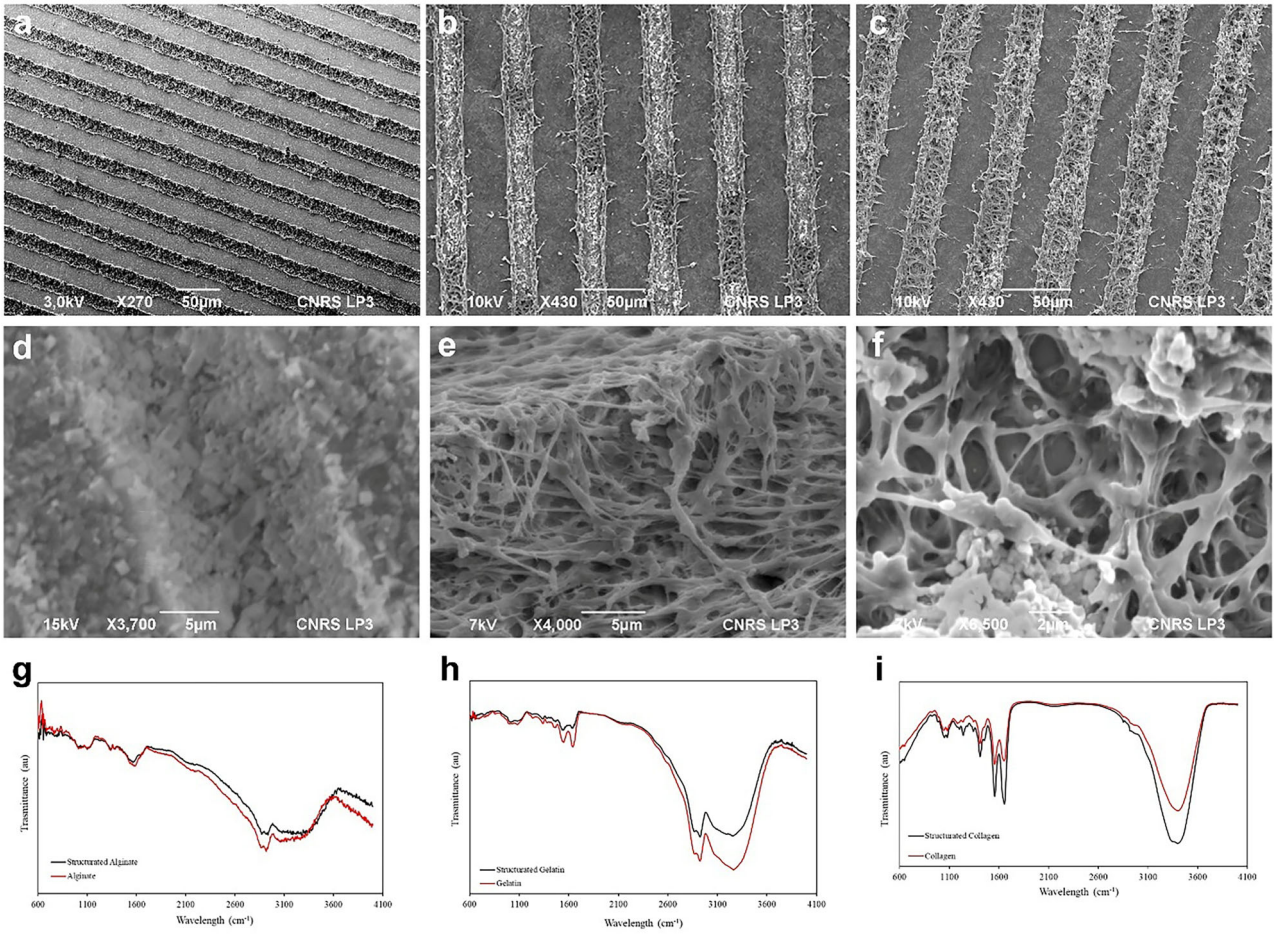

Figure 2. Morphological and chemical characterizations of the structured surfaces; a,d) SEM images of micropatterned surfaces of sodium alginate, b,e) gelatin, and c,f) collagen. g) Infrared spectra for the fine layers of sodium alginate, h) gelatin, and i) collagen. The samples were studied both in their structure and in their initial form.

and 1560 cm^{-1} belongs to the symmetric vibrations of CH_2 and CH_3, while the peaks identified ≈1100 cm^{-1} correspond to the asymmetric C—O and C—O—C stretching vibration. The similarity of the spectra obtained from structured or unstructured samples demonstrates that, at the chosen irradiation conditions, the laser treatment did not cause the appearance of new functional groups that might be potentially toxic for cell survival or growth.

3.3. Study of Coating Suitability for Cell Culture

Once morphologically and chemically characterized, we studied the behavior of the micro-structured supports in a typical cell culture environment. The supports were placed in a 12-well plate, then 2 mL of culture medium containing 5×10^4 cells were added in each well and incubated for 24 h at 37 °C. In these conditions, sodium alginate detached from the glass surface while the structuring process cut the coating layer, resulting in a loss of structural integrity (**Figure** 3a). On the other hand, the gelatin dissolved rapidly in water (less than 1 h) (Figure 3b) while the collagen surface (Figure 3c) was able to maintain its morphology and adhesion throughout the experiment and therefore proved to be the only stable and suitable coating for a long-term study with muscle cells. For this reason, only the collagen-coated supports were used for the following experiments.

Collagen coatings were characterized after laser structuring through confocal (Figure 3d) and SEM (Figure 3e) analysis, which revealed reproducible channels of ≈12–14 µm depth and 25 µm width (Figure 3d,e). Finally, we prepared half-structured coatings in order to study the long-term cell interaction with collagen-coated surfaces and emphasize the effect of laser-induced topography on cell organization. In this regard, channel spacing was adjusted to 35 µm to maximize the processed area. Interestingly, after 3-day of culture, human-immortalized myoblasts displayed signs of organization in the laser-structured compartment (Figure 3f) with a preferential alignment in the direction of the channels.

3.4. Analysis of Myoblast Orientation on Laser Micro-Patterned Surfaces

Myoblast differentiation is an ordered multistep process guided by the stepwise activation of myogenic factors that lead to the

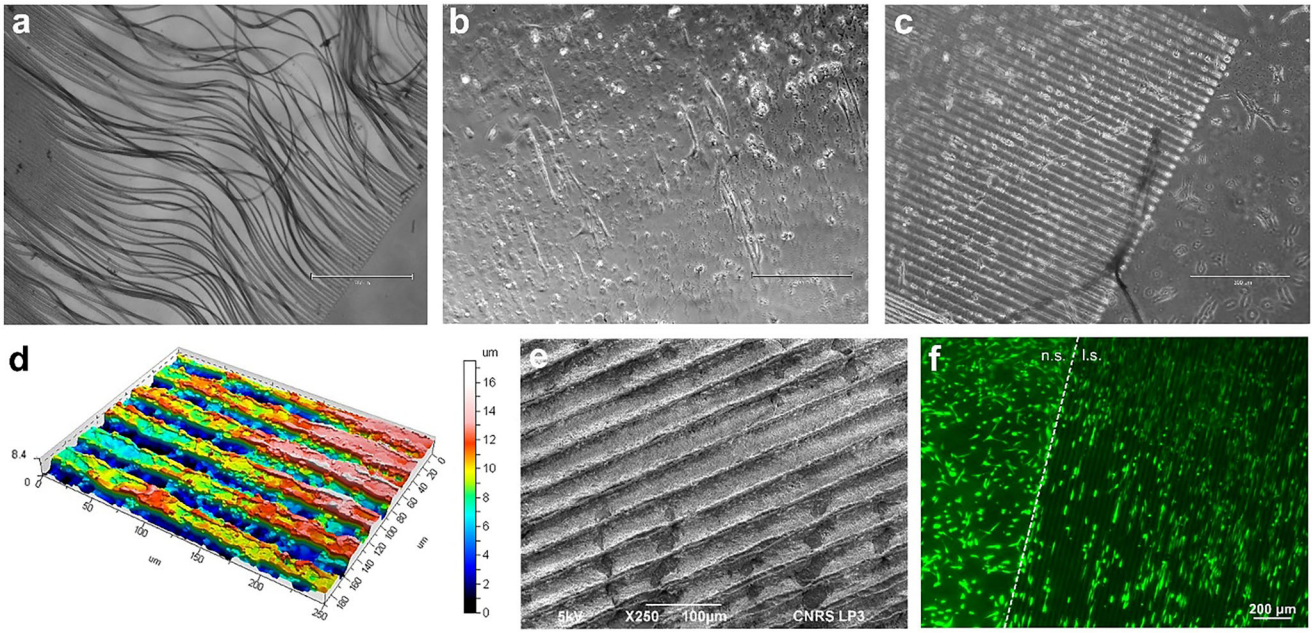

Figure 3. Top: coatings response to the cell culture environment. a) Inverted microscope images of laser-assisted structuring of sodium alginate, b) gelatin, and c) collagen coatings after hydration. Bottom: collagen coating analysis. d) Confocal analysis of the laser-structured collagen-coated surfaces and e) related SEM picture. Human immortalized myoblasts (stained for calcein-AM, green) orientation on non-structured and laser-structured collagen-coated surfaces. The dotted line indicates the boundary between the non-structured and laser-structured areas.

fusion of myoblasts into multinucleated myotubes. Eventually, myotubes will give rise to the diverse muscle fiber types to build the complex skeletal muscle architecture essential to carry out its most important functions, such as body movement, postural behavior, and breathing.[55] The orientation of muscle fibers in vivo is an automatic process driven by the interaction of muscle cells with a well-organized environment and exposure to mechanical forces. In vitro, cells must be guided in adhesion and growth to replicate, once differentiated, the typical organization of human skeletal muscle tissue with parallel aligned muscle fibers.[56] The aim of this study was to promote the orientation of the human myoblasts through an anisotropic surface obtained with the assistance of the laser. To better understand and characterize the previous observations on cell alignment, human immortalized myoblasts were seeded on collagen micro-patterned substrates with different laser-ablated channel spacing (control without structuring, 35, 45, 55, 75, 100, and 150 µm) and cultured for 7 days to allow for myotubes formation.

Myotubes organization was analyzed and we observed an excellent rate of orientation for all the spacing tested (**Figure** 4a–f), as indicated by the presence of a single peak in the graph displaying the distribution of cells in space (Figure 4h). In contrast, myotubes grown on the unstructured control substrates spread randomly without a prevalent orientation (Figure 4g), as shown by the black line in the orientation graph (Figure 4h). For spacing ranging from 35 to 55 µm, we observed a myotube density similar to that of structured channels, with cells grown both within and between channels (Figure 4a–c). As the spacing increased to 75, 100, and 150 µm, the reduction in structured channel density led to a decreased number of myotubes (Figure 4d–f). This observation could be due to the increased area between channels, resulting in reduced geometric constraints on cultured myoblasts. However, even at these higher spacing, sufficient topographical cues are still present to induce preferential orientation (Figure 4h).

Interestingly, a comparison of the myoblast immunostaining pictures with their brightfield counterparts (Figure 4a–g, left half) reveals that at a spacing of 150 µm, the cells do not align with the laser-ablated channel (Figure 4f), despite exhibiting a single orientation peak comparable to the other spacing values (Figure 4h). We concluded that the surface topography at 150 µm can still facilitate the myotubes alignment due to contact geometry, an aspect that should be further investigated by expanding the tested values.

Finally, as shown by the coherency analysis, all tested spacing values were significantly higher than the control, with a maximum of 55 µm (Figure 4i). However, the differences between the individual spacing values were not significant, confirming the effectiveness of the ultrafast laser-induced surface structuring process in creating micro-patterned collagen-coated surfaces capable of guiding muscle cell organization.

3.5. Contact Angle Study on Collagen Layers

To better understand the mechanisms behind cell orientation, the hydrophilicity of the processed collagen surfaces was analyzed through water contact angles (**Figure** 5a). The previously studied spacing values that resulted in controlled cell organization (35, 45, 55, 75, and 100 µm) were chosen to assess the influence of the topography on the surface hydrophilicity. Two measurements were taken, parallel and perpendicular to the

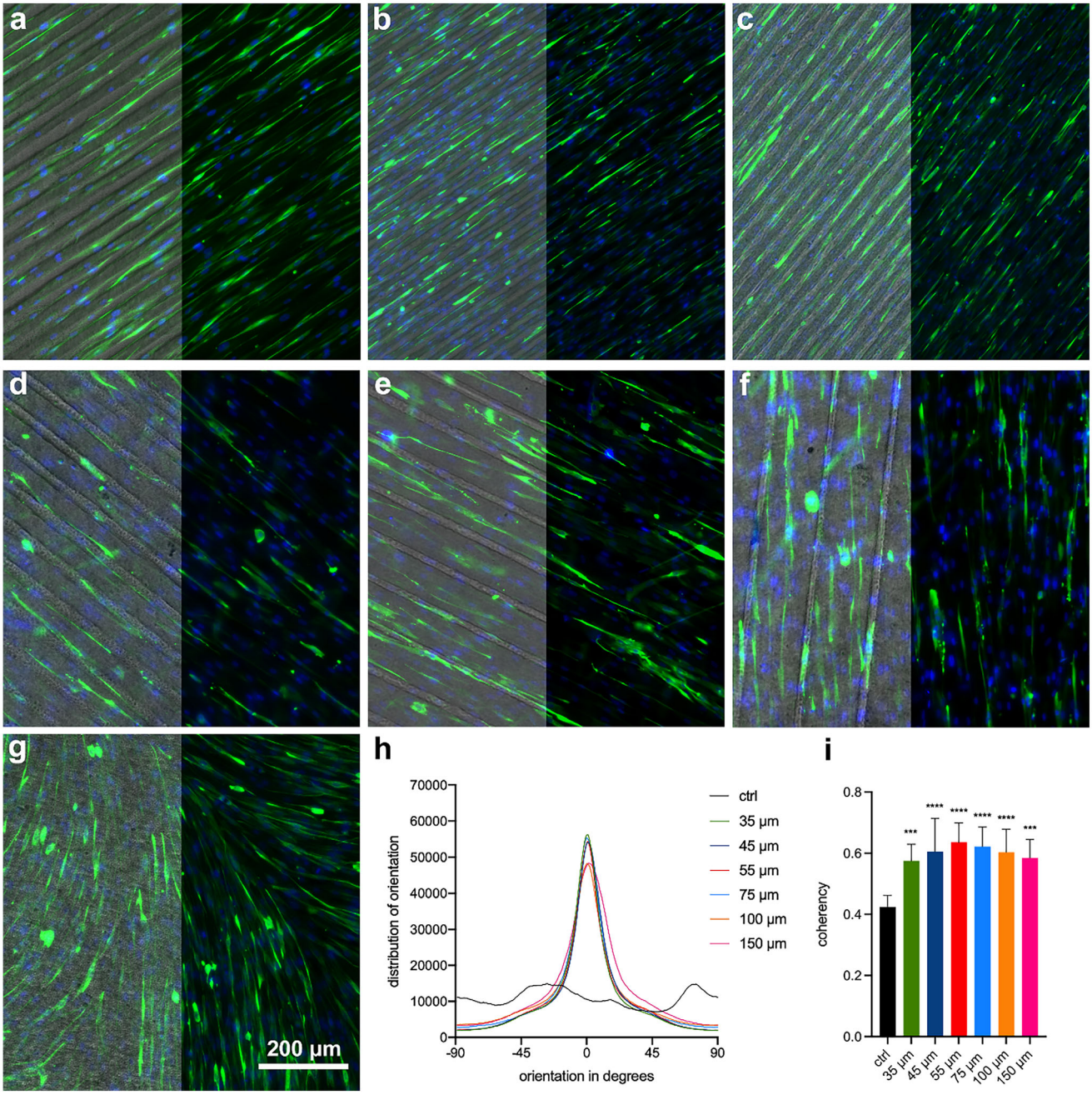

Figure 4. Alignment analysis. Immunofluorescence analysis of human myotubes positive for Desmin (green), juxtaposed with relative brightfield image (left half), grown on collagen-coated laser-structured supports with different spacing values: a) 35 µm, b) 45 µm, c) 55 µm, d) 75 µm, e) 100 µm, f) 150 µm and g) non-structured control. Nuclei are counterstained with Dapi (blue); h) graph of the distribution of orientation for all the experimental conditions and i) the relative coherency values. *P values*: $p = 0001$ (35 µm), $p < 0{,}0001$ (45, 55, 75, and 100 µm), $p = 0004$ (150 µm).

channels. Interestingly, for smaller spacings (35 and 45 µm), the orientation clearly affects the contact angle, with values significantly higher when measurement was done in a perpendicular orientation relative to the channels. Moreover, at these spacing, we found a drastic decrease in the measured contact angles compared to the control, with a minimum reached for 45 µm spacing (Figure 5b). The difference between the structured samples and the control decreased while remaining significant for larger spacings, with values ≈90° and no differences between orientations (Figure 5b).

Studies have demonstrated that the hierarchical structure and porosity in collagen scaffolds enhance the availability of hydroxyl, carboxyl, and amine groups on the scaffold surface. This occurs because porosity and microtopography increase the surface area where these functional groups can interact with the environment, making them more accessible for cellular attachment and

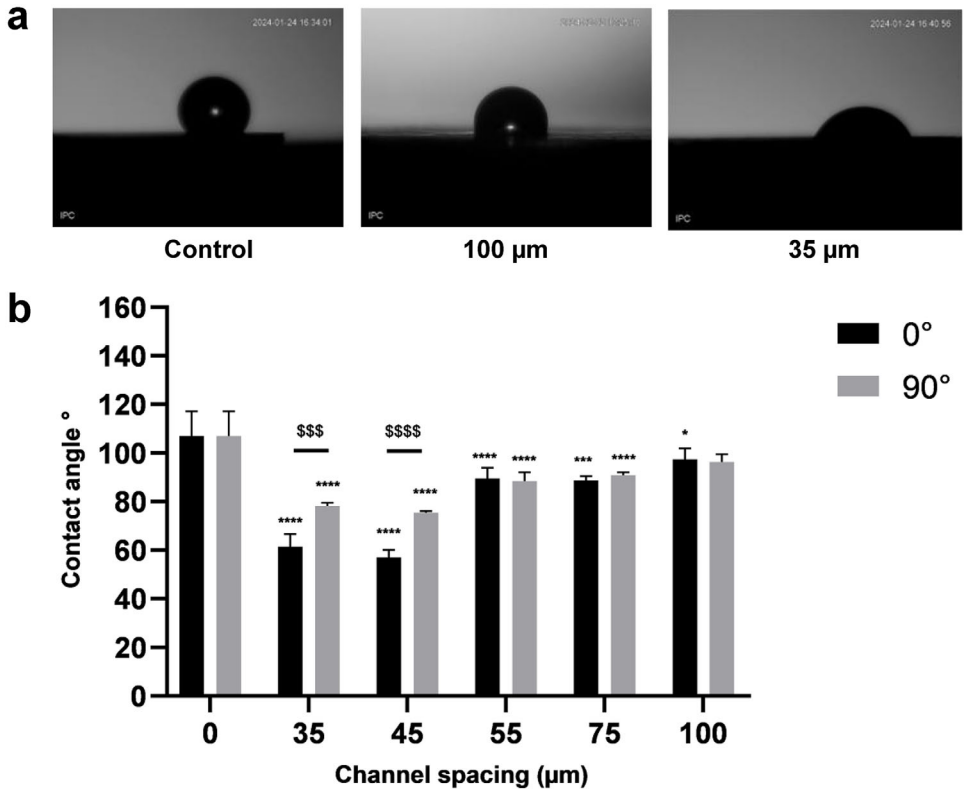

Figure 5. a) Contact angle measurement on structured collagen surfaces at different spacing values. b) Evolution of the contact angle depending on the channel spacing and orientation of the channel, parallel (0°) or perpendicular (90°) to the recording direction. (* compared to control 0°) (p values: **** $p < 0{,}0001$, *** $p = 0{,}0003$, * $p = 0{,}0477$, \$\$\$\$ $p < 0{,}0001$, \$\$\$ $p < 0{,}0002$).

biochemical interactions.[57] In this work, we observed that the increase in surface area due to laser-induced topography and associated porosity (Figure 2c,f) leads to an increase in the amount of exposed polar groups, promoting hydrophilicity (Figure 5b), providing preferential conditions for muscle cells differentiation (Figure 3f). This effect undergoes a natural decay with increased spacing due to a lesser percentage of processed surfaces, ultimately leading to the loss of cell organization (Figure 4f).

4. Conclusion

We report here the application of an ultra-fast laser system to structure the surface of biopolymers. The aim was to develop cell culture supports capable of driving cell growth, orientation, and differentiation in a well-defined and pre-designed structured support.

Different biocompatible biopolymers, such as sodium alginate, gelatin, and collagen, were tested. However, despite the good physico-chemical stability of all three biopolymers during the laser-structuring phase, only the collagen coating proved able to tolerate the biological conditions, being the only one to show stable adhesion to the glass support and excellent resistance to prolonged exposure in the aqueous environment of cell culture conditions.

For this reason, the collagen-coated supports were used to create micro-patterned surfaces thanks to the ultra-fast laser-ablation technique. Anisotropic topographies composed of parallel lines at different spacing (from 35 to 150 µm) were tested for their ability to promote human myoblasts organization. The pattern was specially designed to replicate the skeletal muscle tissue architecture composed of parallel, aligned, and elongated elements corresponding to the muscle fibers. Interestingly, the laser-structured surfaces were able to promote myoblasts organization via contact guidance and to foster their differentiation into highly aligned myotubes. This organization is correlated with the increased hydrophilicity of the substrates following the structuring process for spacing ranging from 35 to 100 µm, as demonstrated by contact angle measurements. Above 100 µm, the density of channels on the collagen surface becomes insufficient to achieve proper control of cell culture conditions.

In conclusion, the reported micro-patterned supports are based on an ultra-fast laser processing of regularly used biocompatible polymers. They integrate seamlessly into the cell culture workflow without additional steps or chemical considerations. Their potentiality was here demonstrated with the alignment of skeletal muscle cells, but their use can easily be extended to other cell types to mimic tissue-specific organization, by varying the spacing and the pattern geometry. The processed surfaces also proved their ability to create well-defined and predesigned cell cultures that can be effectively utilized for skeletal muscle modeling or for the organization of more complex models such as neuromuscular and myotendinous junctions. Finally, the possibility of obtaining well aligned cell culture allows for precise morphological studies with the discrimination of single

independent myotubes. This level of detailed analysis would not be possible with traditional cell culture surfaces where myotubes are randomly oriented (Figure 4g). Given their versatility and ease of integration, laser micro-patterned supports represent a powerful tool for tissue engineering and biomedical applications.

Acknowledgements

C.M. and L.D. contributed equally to this work. The work was funded by the French National Research Agency (ANR Medilibs and Diagem projects) together with the French Defense Innovation Agency (ANR—DGA/AID—ICELARE Project ID ANR—20—ASTR—0004). The PhD thesis of Lucas Duvert was co-funded by Aix-Marseille University, the French Defense Innovation Agency, and the MarMaRa funding scheme. This work received support from the French government under the France 2030 investment plan, as part of the Initiative d'Excellence d'Aix-Marseille Université – A*MIDEX "AMX-23-CPJ-05." The project leading to this publication has received funding from the Excellence Initiative of Aix-Marseille University-A*Midex, a French "Investissement d'avenir program" AMX-19-IET-007, through the MarMaRa funding scheme. This work was conducted using LaMP facilities at LP3. The authors also acknowledge the "Region SUD" for their financial support.

Conflict of Interest

The authors declare no conflict of interest.

Data Availability Statement

The data that support the findings of this study are available from the corresponding author upon reasonable request.

Keywords

biomaterials, contact guidance, laser direct writing, muscle tissue engineering, surface structuring

Received: February 12, 2025
Revised: March 31, 2025
Published online: May 8, 2025

[1] S. Testa, M. Costantini, E. Fornetti, S. Bernardini, M. Trombetta, D. Seliktar, S. Cannata, A. Rainer, C. Gargioli, *J. Cell. Mol. Med.* **2017**, *21*, 2711.
[2] H. Kim, M.-C. Kim, H. H. Asada, *Sci. Rep.* **2019**, *9*, 2732.
[3] J. Na, C. Tai, Z. Wang, Z. Yang, X. Chen, J. Zhang, L. Zheng, Y. Fan, *Biomaterials* **2025**, *312*, 122715.
[4] L. Rijns, M. G. T. A. Rutten, A. F. Vrehen, A. A. Aldana, M. B. Baker, P. Y. W. Dankers, *Nanoscale* **2024**, *16*, 16290.
[5] J. R. Libby, H. Royce, S. R. Walker, L. Li, *Biomater. Biosyst.* **2024**, *15*, 100097.
[6] L. Papadimitriou, A. Karagiannaki, E. Stratakis, A. Ranella, *Mechanobiol. Med.* **2024**, *2*, 100039.
[7] F. Martino, A. R. Perestrelo, V. Vinarský, S. Pagliari, G. Forte, *Front. Physiol.* **2018**, *9*, 824.
[8] C. Y. Guo, R. Mo, H. Kim, *J. Oral Biol. Craniofac. Res.* **2024**, *14*, 471.
[9] M. Cong, X. Wu, L. Zhu, G. Gu, F. Ding, G. Li, H. Shi, *Regen. Biomater.* **2024**, *11*, rbae005.
[10] A. Lecomte, A. Casanova, M.-C. Blatché, J. Gonzalès, A. Ajagli, L. Mazenq, D. Gonzalez-Dunia, G. Larrieu, **2024**, *9*.
[11] V. Errico, G. Arrabito, E. Fornetti, C. Fuoco, S. Testa, G. Saggio, S. Rufini, S. Cannata, A. Desideri, C. Falconi, C. Gargioli, *ACS Appl. Mater. Interfaces* **2018**, *10*, 14097.
[12] G. H. Yang, J. Lee, G. Kim, *Biofabrication* **2019**, *11*, 025005.
[13] Y. Nishimura, K. Yano, M. Itoh, M. Ito, *Flat Panel Display Manufacturing*, (Eds: J. Souk, S. Morozumi, F.-C. Luo, I. Bita), John Wiley & Sons, Ltd, Hoboken, New Jersey, USA **2018**, pp. 287–310.
[14] J. L. Charest, A. J. García, W. P. King, *Biomaterials* **2007**, *28*, 2202.
[15] N. Kaga, R. Horiuchi, A. Yokoyama, T. Akasaka, Y. Yoshida, *e-J. Surf. Sci. Nanotech.* **2017**, *15*, 1.
[16] M. Patel, S. Ahn, W.-G. Koh, *J. Ind. Eng. Chem.* **2022**, *114*, 19.
[17] T. Limongi, L. Brigo, L. Tirinato, F. Pagliari, A. Gandin, P. Contessotto, A. Giugni, G. Brusatin, *Biomed. Mater.* **2021**, *16*, 035013.
[18] H. Sariogullari, A. Z. Aroguz, Z. Adiguzel, *Mol. Biotechnol.* **2023**, *65*, 786.
[19] A. Casanova, M.-C. Blatche, C. A. Ferre, H. Martin, D. Gonzalez-Dunia, L. Nicu, G. Larrieu, *Langmuir* **2018**, *34*, 6612.
[20] D. Qin, Y. Xia, G. M. Whitesides, *Nat. Protoc.* **2010**, *5*, 491.
[21] Y. Xia, G. M. Whitesides, *Angew. Chem., Int. Ed.* **1998**, *37*, 550.
[22] X. Liu, A. Zanut, M. Sladkova-Faure, L. Xie, M. Weck, X. Zheng, E. Riedo, G. M. de Peppo, *Adv. Funct. Mater.* **2021**, *31*, 2008662.
[23] S. Fruncillo, X. Su, H. Liu, L. S. Wong, *ACS Sens.* **2021**, *6*, 2002.
[24] A. Riveiro, A. L. B. Maçon, J. del Val, R. Comesaña, J. Pou, *Front. Phys.* **2018**, *6*.
[25] E. Stratakis, A. Ranella, M. Farsari, C. Fotakis, *Prog. Quantum Electron.* **2009**, *33*, 127.
[26] A. A. Antoshin, S. N. Churbanov, N. V. Minaev, D. Zhang, Y. Zhang, A. I. Shpichka, P. S. Timashev, *Bioprinting* **2019**, *15*, 00052.
[27] J. Chang, X. Sun, *Front. Bioeng. Biotechnol.* **2023**, *11*, 1255782.
[28] M. Malinauskas, M. Farsari, A. Piskarskas, S. Juodkazis, *Phys. Rep.* **2013**, *533*, 1.
[29] V. Harinarayana, Y. C. Shin, *Opt. Laser Technol.* **2021**, *142*, 107180.
[30] V. Dinca, L. E. Sima, L. Rusen, A. Bonciu, T. Lippert, M. Dinescu, M. Farsari, *Recent Advances in Biopolymers*, (Ed: F. K. Parveen), InTech, London, UK **2016**.
[31] E. Rebollar, J. Mildner, N. Götte, D. Otto, C. Sarpe, J. Köhler, M. Wollenhaupt, T. Baumert, M. Castillejo, *Appl. Surf. Sci.* **2014**, *302*, 231.
[32] Z. K. Wang, H. Y. Zheng, C. P. Lim, Y. C. Lam, *Appl. Phys. Lett.* **2009**, *95*, 111110.
[33] P. Shukla, D. G. Waugh, J. Lawrence, R. Vilar, *Laser Surface Modification of Biomaterials*, Elsevier, Amsterdam, Netherlands **2016**, pp. 281–299.
[34] B. Neuenschwander, B. Jaeggi, M. Schmid, G. Hennig, *Phys. Procedia* **2014**, *56*, 1047.
[35] D. Angelaki, P. Kavatzikidou, C. Fotakis, E. Stratakis, A. Ranella, *Mater. Sci. Eng., C* **2020**, *115*, 111144.
[36] N. Pien, H. Krzyslak, S. Shastry Kallaje, J. Van Meerssche, D. Mantovani, C. De Schauwer, P. Dubruel, S. Van Vlierberghe, C. P. Pennisi, *Appl. Mater. Today* **2023**, *31*, 101737.
[37] R. Hashiguchi, H. Ichikawa, M. Kumeta, D. Koyama, *Sci. Rep.* **2024**, *14*, 25737.
[38] R. Ahmad Raus, W. M. F. Wan Nawawi, R. R. Nasaruddin, *Asian J Pharm. Sci.* **2021**, *16*, 280.
[39] N. Farshidfar, S. Iravani, R. S. Varma, *Mar. Drugs.* **2023**, *21*, 189.
[40] Y. He, C. Wang, C. Wang, Y. Xiao, W. Lin, *Polymers* **2021**, *13*, 2299.
[41] Y. Piao, H. You, T. Xu, H.-P. Bei, I. Z. Piwko, Y. Y. Kwan, X. Zhao, *Eng. Regener.* **2021**, *2*, 47.
[42] S. Sethi, Medha, B. S. Kaith, *React. Funct. Polym.* **2022**, *179*, 105362.
[43] W. Peng, D. Li, K. Dai, Y. Wang, P. Song, H. Li, P. Tang, Z. Zhang, Z. Li, Y. Zhou, C. Zhou, *Int. J. Biol. Macromol.* **2022**, *208*, 400.
[44] T. A. T. Araujo, M. C. Almeida, I. Avanzi, J. Parisi, A. F. Simon Sales, Y. Na, A. Renno, *J. Biomater. Appl.* **2021**, *36*, 95.

[45] F. Wehrhan, E. Nkenke, I. Melnychenko, K. Amann, K. A. Schlegel, C. Goerlach, W.-H. Zimmermann, S. Schultze-Mosgau, *Dermatol. Surg.* **2010**, *36*, 919.
[46] N. Ray, T. van Noorden, F. Radu, W. Friess, P. Knabner, *ZAMM – J. Appl. Math. Mech./Zeitschrift für Angewandte Mathematik und Mechanik* **2013**, *93*, 811.
[47] J. D. Robin, W. E. Wright, Y. Zou, S. C. Cossette, M. W. Lawlor, E. Gussoni, *J. Vis. Exp.* **2015**, *18*, 52307.
[48] J. M. Liu, *Opt. Lett.* **1982**, *7*, 196.
[49] M. Brugnara, *ImageJ. nih* **2006**.
[50] C. Murru, L. Duvert, F. Magdinier, A. Casanova, A.-P. Alloncle, S. Testa, A. Al-Kattan, *Nanoscale Adv.* **2024**, *6*, 2104.
[51] Z. Püspöki, M. Storath, D. Sage, M. Unser, in *Focus on Bio-Image Informatics*, (Eds: W. H. De Vos, S. Munck, J.-P. Timmermans), Springer International Publishing, Cham, Germany **2016**, pp. 69–93.
[52] J. Schindelin, I. Arganda-Carreras, E. Frise, V. Kaynig, M. Longair, T. Pietzsch, S. Preibisch, C. Rueden, S. Saalfeld, B. Schmid, J.-Y. Tinevez, D. J. White, V. Hartenstein, K. Eliceiri, P. Tomancak, A. Cardona, *Nat. Methods* **2012**, *9*, 676.
[53] M. Costantini, S. Testa, P. Mozetic, A. Barbetta, C. Fuoco, E. Fornetti, F. Tamiro, S. Bernardini, J. Jaroszewicz, W. Święszkowski, M. Trombetta, L. Castagnoli, D. Seliktar, P. Garstecki, G. Cesareni, S. Cannata, A. Rainer, C. Gargioli, *Biomaterials* **2017**, *131*, 98.
[54] L. Terrie, M. Burattini, S. Van Vlierberghe, L. Fassina, L. Thorrez, *Front. Bioeng. Biotechnol.* **2022**, *10*, 892287.
[55] D. Cretoiu, L. Pavelescu, F. Duica, M. Radu, N. Suciu, S. M. Cretoiu, *Adv. Exp. Med. Biol.* **2018**, *1088*, 23.
[56] F. Yusuf, B. Brand-Saberi, *Histochem. Cell Biol.* **2012**, *138*, 187.
[57] M. Moncayo-Donoso, G. A. Rico-Llanos, D. A. Garzón-Alvarado, J. Becerra, R. Visser, M. R. Fontanilla, *Polymers* **2021**, *13*, 3187.